2017

Amorphous protein aggregates stimulate plasminogen activation, leading to release of cytotoxic fragments that are clients for extracellular chaperones

Patrick Constantinescu
University of Wollongong, pac576@uowmail.edu.au

Rebecca Brown
University of Wollongong, rab772@uowmail.edu.au

Amy R. Wyatt
University of Wollongong, awyatt@uow.edu.au

Marie Ranson
University of Wollongong, mranson@uow.edu.au

Mark R. Wilson
University of Wollongong, mrw@uow.edu.au

Publication Details

Constantinescu, P., Brown, R. A., Wyatt, A. R., Ranson, M. & Wilson, M. R. (2017). Amorphous protein aggregates stimulate plasminogen activation, leading to release of cytotoxic fragments that are clients for extracellular chaperones. Journal Of Biological Chemistry, 292 (35), 14425-14437.

Amorphous protein aggregates stimulate plasminogen activation, leading to release of cytotoxic fragments that are clients for extracellular chaperones

Abstract

The misfolding of proteins and their accumulation in extracellular tissue compartments as insoluble amyloid or amorphous protein aggregates are a hallmark feature of many debilitating protein deposition diseases such as Alzheimer's disease, prion diseases, and type II diabetes. The plasminogen activation system is best known as an extracellular fibrinolytic system but was previously reported to also be capable of degrading amyloid fibrils. Here we show that amorphous protein aggregates interact with tissue-type plasminogen activator and plasminogen, via an exposed lysine-dependent mechanism, to efficiently generate plasmin. The insoluble aggregate-bound plasmin is shielded from inhibition by α_2-antiplasmin and degrades amorphous protein aggregates to release smaller, soluble but relatively hydrophobic fragments of protein (plasmin-generated protein fragments (PGPFs)) that are cytotoxic. In vitro, both endothelial and microglial cells bound and internalized PGPFs before trafficking them to lysosomes. Clusterin and α_2-macroglobulin bound to PGPFs to significantly ameliorate their toxicity. On the basis of these findings, we hypothesize that, as part of the in vivo extracellular proteostasis system, the plasminogen activation system may work synergistically with extracellular chaperones to safely clear large and otherwise pathological protein aggregates from the body.

Disciplines

Medicine and Health Sciences

Publication Details

Constantinescu, P., Brown, R. A., Wyatt, A. R., Ranson, M. & Wilson, M. R. (2017). Amorphous protein aggregates stimulate plasminogen activation, leading to release of cytotoxic fragments that are clients for extracellular chaperones. Journal Of Biological Chemistry, 292 (35), 14425-14437.

Amorphous protein aggregates stimulate plasminogen activation, leading to release of cytotoxic fragments that are clients for extracellular chaperones

Received for publication, March 22, 2017, and in revised form, May 9, 2017 Published, Papers in Press, July 14, 2017, DOI 10.1074/jbc.M117.786657

Patrick Constantinescu[1], **Rebecca A. Brown**[1], **Amy R. Wyatt**[2], **Marie Ranson, and Mark R. Wilson**[3]

From the Illawarra Health and Medical Research Institute, Proteostasis and Disease Research Centre, and the School of Biological Sciences, University of Wollongong, Northfields Avenue, Wollongong, New South Wales 2522, Australia

Edited by George N. DeMartino

The misfolding of proteins and their accumulation in extracellular tissue compartments as insoluble amyloid or amorphous protein aggregates are a hallmark feature of many debilitating protein deposition diseases such as Alzheimer's disease, prion diseases, and type II diabetes. The plasminogen activation system is best known as an extracellular fibrinolytic system but was previously reported to also be capable of degrading amyloid fibrils. Here we show that amorphous protein aggregates interact with tissue-type plasminogen activator and plasminogen, via an exposed lysine-dependent mechanism, to efficiently generate plasmin. The insoluble aggregate-bound plasmin is shielded from inhibition by α_2-antiplasmin and degrades amorphous protein aggregates to release smaller, soluble but relatively hydrophobic fragments of protein (plasmin-generated protein fragments (PGPFs)) that are cytotoxic. *In vitro*, both endothelial and microglial cells bound and internalized PGPFs before trafficking them to lysosomes. Clusterin and α_2-macroglobulin bound to PGPFs to significantly ameliorate their toxicity. On the basis of these findings, we hypothesize that, as part of the *in vivo* extracellular proteostasis system, the plasminogen activation system may work synergistically with extracellular chaperones to safely clear large and otherwise pathological protein aggregates from the body.

We previously identified a number of abundant extracellular chaperones (ECs)[4] found in body fluids that have the ability to specifically bind to exposed regions of hydrophobicity on misfolded proteins to inhibit their toxicity and facilitate their safe clearance and disposal. This is relevant to a broad variety of serious human diseases, the protein deposition diseases, in which pathology is associated with inappropriate misfolding, aggregation, and deposition of extracellular proteins (*e.g.* Alzheimer's disease, type II diabetes, prion diseases, etc.). The clearance mechanism is thought to involve ECs forming soluble complexes with misfolded proteins (or oligomers) and the delivery of these to cell surface receptors for uptake and subsequent lysosomal degradation (1). Acting alone, however, these systems are not capable of clearing large, insoluble extracellular protein deposits that are associated with pathology in, for example, systemic amyloidosis and rheumatoid arthritis. Nevertheless, following successful clinical treatment, the extracellular tissue deposits that characterize these diseases measurably regress (2), implying that the body does have an effective mechanism(s) to clear large, insoluble protein deposits from extracellular spaces. Obvious candidates for involvement in such systems are extracellular proteases, in particular those that can be specifically activated by protein aggregates. Conceivably, proteases such as this could digest insoluble extracellular protein aggregates to generate smaller, soluble protein fragments that are more amenable to clearance, potentially via the same EC-facilitated mechanisms implicated in clearing soluble misfolded proteins/oligomers (as proposed in Ref. 1).

The plasminogen activation system (PAS) is a suitable candidate extracellular protease system that may contribute to the degradation of insoluble extracellular protein deposits *in vivo*. The PAS includes many proteolytic enzymes with functions ranging from tumor invasion and metastasis, tissue remodeling (3, 4), and reproduction (5) to the inflammatory response (6) and hemostasis (7). It includes the major protease plasmin (plm; a broad spectrum serine protease), plasminogen (plg; the zymogen form of plm), specific mammalian plg activators, urokinase-type plg activator, and tissue-type plg activator (tPA) as well as plg activator inhibitors type-1 and -2 and inhibitors of plasmin such as α_2-antiplasmin (A2AP) and α_2-macroglobulin (A2M) (3, 4). Plm degrades fibrin and fibrinogen with the highest specificity; termed fibrinolysis, this process is important for wound healing and hemostasis (8). When both tPA and plg bind to fibrin, tPA cleaves plg to generate active plm, leading to dissolution of macromolecular fibrin clots. Interestingly, it has been reported that plasmin digestion of fibrin yields several

The authors declare that they have no conflicts of interest with the contents of this article.

This article contains supplemental Figs. 1–5.

[1] Recipients of Australian Government postgraduate awards.

[2] Supported by Australian National Health and Medical Research Council Early Career Fellowship GNT1012521.

[3] Supported by Australian Research Council Grant DP160100011. To whom correspondence should be addressed: School of Biological Sciences, Illawarra Health and Medical Research Institute (IHMRI), Bldg. 32, University of Wollongong, Northfields Ave., Wollongong, NSW 2522, Australia. Tel.: 61-2-42214534; Fax: 61-2-42218130; E-mail: mrw@uow.edu.au.

[4] The abbreviations used are: EC, extracellular chaperone; PGPF, plasmin-generated protein fragment; PAS, plasminogen activation system; plm, plasmin; plg, plasminogen; tPA, tissue-type plg activator; A2AP, α_2-antiplasmin; A2M, α_2-macroglobulin; Aβ, amyloid β; OVO, ovotransferrin; SOD, superoxide dismutase 1; bisANS, 4,4′-bis(1-anilino-8-naphthalene sulfonate); Thio-T, thioflavin T; TXA, tranexamic acid; M-β-CD, methyl-β-cyclodextrin; CLU, clusterin; MTS, 3-(4,5-dimethylthiazol-2-yl)-5-(3-carboxymethoxyphenyl)-2-(4-sulfophenyl)-2*H*-tetrazolium; SH3, Src homology 3; Tricine, *N*-[2-hydroxy-1,1-bis(hydroxymethyl)ethyl]glycine; SPEC-PL, SPECTROZYME PL; Tx-100, Triton X-100; HDC, heat-denatured casein.

specific proteolytic fragments, including a cytotoxic "fibrin fragment E," which induces apoptosis in a variety of cell types (9).

The PAS is also known to be activated by aggregated amyloid β, the peptide that forms insoluble plaques in the brains of Alzheimer's disease patients, and plm degrades fibrillar Aβ with physiologically relevant efficiency (10). Previous work suggests that tPA binds to both fibrin and amyloid proteins by recognizing cross-β-sheet structure (11). Cross-β-sheet structure may promote the interaction between tPA and plg, resulting in plm-mediated degradation of β-sheet-rich proteins independent of their amino acid sequence (11, 12). Other proteins known to activate the PAS include prion protein (14), extracellular matrix proteins, actin, glycated proteins, and thrombospondin (4). Furthermore, several earlier reports have described plg activation by a wide range of denatured proteins but not by the corresponding native proteins (15–17). These denatured proteins were not structurally characterized, but the harsh conditions used to generate them (*e.g.* extremes of pH and temperature (15, 17)) are likely to have mostly resulted in the formation of unstructured amorphous protein aggregates. Injured cells with damaged cell membranes also release protein aggregates that induce tPA-mediated plm formation, facilitating removal of the aggregates by proteolytic degradation (12). The aggregates examined in the latter study were shown to stain with thiazine red R and Congo red, indicating that they were rich in β-sheet content, but were otherwise not structurally characterized (12).

Although previous work has identified that denatured proteins, but not the corresponding native proteins, can induce plg activation to plm, there has been limited characterization of the structural features responsible for this activity. Furthermore, although the products of plm digestion of fibrin clots have certainly been studied (9, 18), the corresponding plm digestion products of amorphous protein aggregates had not been examined. In the current study, we generated and biophysically characterized amorphous aggregates from ovotransferrin (OVO) and the G93A mutant of superoxide dismutase 1 (SOD) and confirmed that they act as efficient cofactors for the PAS. We then characterized the products of plm-mediated digestion of the amorphous aggregates as hydrophobic and cytotoxic protein fragments (peptides) of varying size that are internalized by cells and that are specifically bound by ECs, which inhibits their toxicity. These results are consistent with a hypothetical model in which the collective *in vivo* activities of ECs and the PAS may help safely clear large and otherwise pathological protein aggregates from the body.

Results

Generation and characterization of aggregates of SOD and OVO

The G93A mutant of SOD and OVO were subjected to chemical reduction (50 mM DTT for 24 h at 37 °C) or heat (60 °C for 2 h), respectively, to induce protein aggregation. SOD is capable of generating fibrillar aggregates under conditions similar to those used here, but this process is often difficult to reproduce *in vitro* (19). In our hands, using the method described, recombinant SOD produced amorphous aggregates. The generation of amorphous OVO aggregates using the conditions described has been reported previously (20). When treated in this way, the two proteins showed a time-dependent increase in exposed hydrophobicity, detected by 4,4′-bis(1-anilino-8-naphthalene sulfonate) (bisANS) fluorescence, which plateaued at later stages of the time course (Fig. 1, *A* and *B*). Similarly, after a short lag phase, the turbidity (A_{360}) of the protein solutions quickly increased before also plateauing at the later stages of the time course (Fig. 1, *A* and *B*). These results suggest that the conditions used first induce misfolding of the protein molecules associated with an increase in regions of exposed hydrophobicity and then a time-dependent association of the misfolded species to form increasingly large, light-scattering aggregates. Thioflavin T fluorescence analyses indicated that the aggregates formed did not contain significant quantities of cross-β-sheet content and were therefore not amyloid in structure (Fig. 1*C*). Scanning electron microscopy of the end point aggregates indicated in both cases an amorphous structure lacking fibrillar content (Fig. 1*D*).

Amorphous protein aggregates stimulate activation of plg to plm by a lysine-dependent mechanism and protect plm from inhibition by A2AP

Fibrin stimulated the fastest initial rate of change of plm activity with mean values of $0.101 \pm 0.030\ \Delta A_{405}{\cdot}\text{min}^{-2}$ ($n = 9$). This equated to an average -fold increase of $\sim 7.1 \pm 1.7$ compared with tPA/plg alone across three independent assays (Fig. 2, *A* and *B*). When also expressed as a -fold increase in initial rate of change of plm activity compared with tPA/plg alone, both amorphous protein aggregates gave a similar mean -fold increase of 2.5 ± 0.4 across three independent assays (Fig. 2, *A* and *B*). This suggests that, analogous to fibrin, amorphous aggregates likely co-localize tPA and plg, thereby acting as a cofactor to increase the rate of activation of plg to plm. The extent of plg activation was dependent on the amount of amorphous aggregate present; early time point samples from protein aggregation mixtures, which contained fewer large aggregates, elicited lower levels of plm activation (supplemental Fig. 1). The results of related experiments confirmed that activation of the tPA/plg system by amorphous protein aggregates is not exclusive to SOD and OVO (supplemental Fig. 2). The binding of tPA and plg to fibrin is lysine-dependent. It was previously reported that this was also a requirement for the activation of plg by denatured proteins (16). The lysine-like analogue tranexamic acid (TXA) is commonly used to confirm the lysine-dependent binding of plg to various ligands and receptors (4). We showed that TXA significantly inhibited the ability of SOD aggregates and fibrin (as an intra-assay cofactor control) to elicit plg activation by ~47 and ~64%, respectively, compared with no-TXA controls (Fig. 2*C*). Similarly, TXA significantly inhibited OVO- and fibrin-mediated plg activation by ~90 and ~86%, respectively (Fig. 2*D*). These results confirm an important role for lysine residues in the interaction between amorphous protein aggregates and tPA/plg.

In mammalian plasma, A2AP is the main physiologic plm inhibitor; it acts by rapidly forming a 1:1 stoichiometric complex with the protease (21–23). For plm to perform its primary

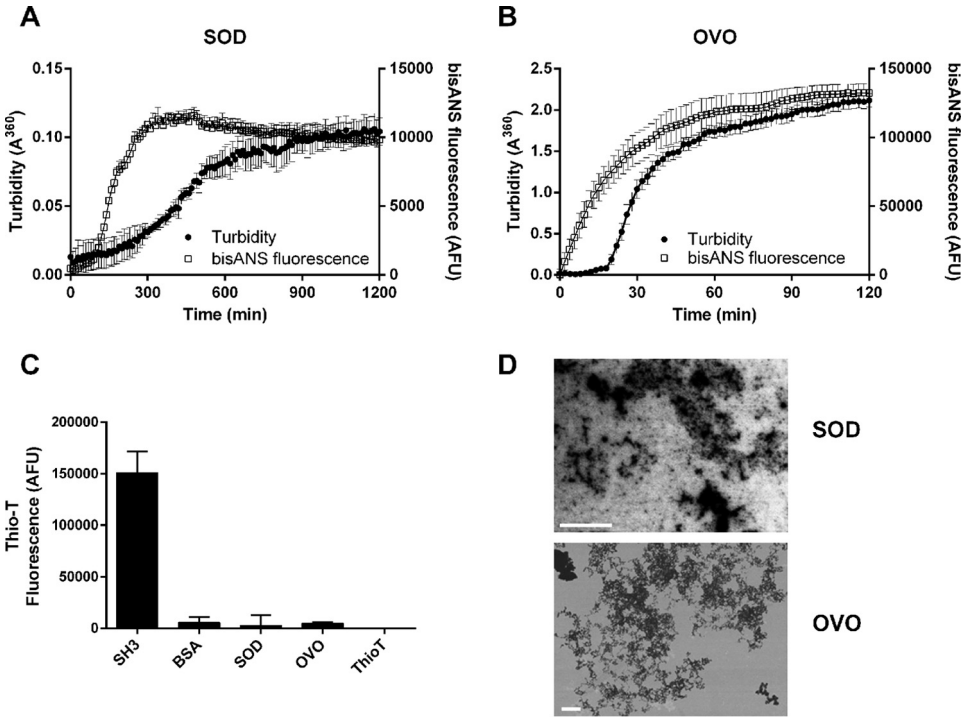

Figure 1. Heat or chemical stress induces increased exposed hydrophobicity and aggregation of SOD and OVO into β-sheet-poor, non-fibrillar amorphous aggregates. SOD (*A*) and OVO (*B*) were induced to aggregate as described under "Experimental procedures." Exposed hydrophobicity and aggregation were measured as changes in relative bisANS-associated fluorescence (*AFU*) and turbidity (A_{360}) over time, respectively. *C*, Thio-T was incubated in the absence or presence of samples (5 μM) of either SOD or OVO aggregates taken postaggregation (300 and >34 min, respectively) or control proteins, and the level of β-sheet content was measured as the relative Thio-T fluorescence intensity. Fibrillar aggregates of SH3 and native BSA were used as positive and negative control proteins, respectively. Data points in *A–C* represent the mean of three separate experiments, each performed in triplicate ($n = 9$; *error bars* represent S.E.). *D*, representative scanning electron micrographs of SOD and OVO aggregates taken postaggregation (300 and 34 min, respectively). Amorphous aggregates are present. *White scale bars* represent 1 μm.

role, the efficient dissolution of fibrin clots, it is sterically protected when bound to fibrin from inhibition by A2AP (24). Inhibition by A2AP requires the presence of a free active site and free lysine-binding sites in plg/plm; these are inaccessible when plg/plm is bound to substrates such as fibrin (21–23). We tested whether or not plm was also protected from A2AP inhibition when bound to amorphous protein aggregates. We first separated end point aggregation mixtures of SOD and OVO by centrifugation (15,000 × *g* for 30 min) into fractions designated as soluble and insoluble before separately testing them in the colorimetric plg activation assay with and without A2AP. The soluble fraction would be expected to contain a mixture of small aggregates and monomeric protein molecules, whereas the insoluble fraction would contain large protein aggregates. For SOD and OVO, both the soluble and insoluble fractions elicited significant plg activation (supplemental Fig. 1). Although A2AP inhibited ~70–75% of the plm activity generated by soluble protein fractions, it was only able to inhibit ~27–42% of the corresponding activity elicited by insoluble protein fractions (Fig. 2, *E* and *F*). Thus, when associated with large, insoluble amorphous protein aggregates, plm is relatively resistant to inhibition by A2AP.

Plasmin digests amorphous protein aggregates to generate heterogeneously sized and hydrophobic protein fragments

Amorphous protein aggregates prepared as described above were digested with plm to generate soluble fragments (amorphous aggregate-derived plasmin-generated protein fragments (^{amorph}PGPFs)), which were then analyzed together with whole (undigested) protein aggregates by reducing SDS-PAGE. Native proteins were also digested with plm under the same conditions to generate experimental controls (^{native}PGPFs). Most of the SOD and OVO aggregates were too large to enter the SDS-polyacrylamide gel and accumulated at the top of the resolving gel (Fig. 3*A*). Other minor species that entered the gel are likely to represent smaller aggregates. The digestion of aggregated SOD yielded ^{amorph}PGPFs ranging in size from 15 to 200 kDa that appeared as a smear with no visually distinct bands. Digestion of aggregated OVO yielded ^{amorph}PGPFs ranging in size from 88 to 164 kDa and a smear of other visually indistinct bands less than 75 kDa in size. Autolysis of plm resulting from prolonged incubation (>2 h at neutral pH) in aqueous solution was evident based on the fact that bands corresponding to plm heavy chain (~63 kDa) and light chain (~26.5 kDa) (25) are not easily visually resolved from those detected in PGPF preparations. PGPFs, together with their parent proteins/aggregates and other controls, were also analyzed for exposed hydrophobicity in a bisANS fluorescence assay (Fig. 3*B*). In all cases, aggregates and their corresponding ^{amorph}PGPFs, but not native proteins or the corresponding ^{native}PGPFs, had significantly higher bisANS fluorescence than wells containing only bisANS (Fig. 3*B*). Additionally, amorphous protein aggregates had ~30% greater bisANS fluorescence than the corresponding ^{amorph}PGPFs (a significant difference). Relative to bisANS alone, SOD aggregates and

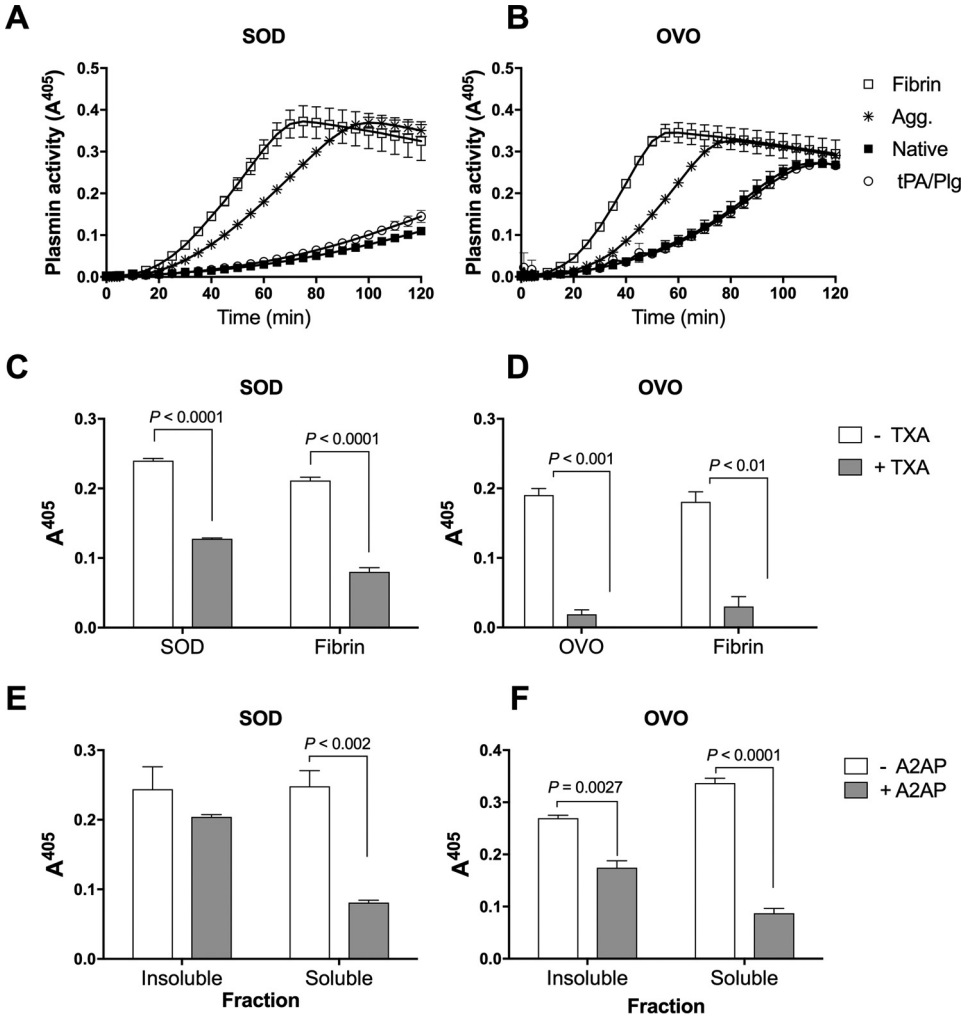

Figure 2. Plg activation assays. *A* and *B*, aggregated or native non-aggregated protein sample or fibrin as a positive control (all at 75 μg/m) were preincubated in the presence of 250 nM plg and 500 nM SPEC-PL. The reaction was initiated by the addition of 5 nM tPA, and the change in A_{405} was recorded. tPA/plg alone and fibrin served as controls for plg activation in the absence or presence of cofactor, respectively. Data points represent the mean of three separate experiments, each performed in triplicate ($n = 9$; *error bars* represent S.E.). *C–F*, bar graphs showing results from other assays in which protein aggregates (*C* and *D*) or soluble and insoluble fractions prepared from aggregation mixtures (*E* and *F*) (all at 75 μg/ml) were incubated first for 30 min with 5 nM tPA and 250 nM plg and then for 15 min with or without specific inhibitors (*C* and *D*, 10 mM TXA; *E* and *F*, 400 nM A2AP) before adding the plm substrate and measuring changes in A_{405} as described previously. Data shown are means of three replicates (*error bars* represent S.D.) and correspond to 120-min time points, which in these assays were when the A_{405} had reached a maximum. Significant differences are indicated. The results shown are representative of two independent experiments. *Agg.*, aggregates.

^{amorph}PGPFs had, respectively, ~2.7- and ~2.1-fold greater bisANS fluorescence. The corresponding values for OVO aggregates and ^{amorph}PGPFs were ~3.5- and ~2.8-fold, respectively. The fluorescence of wells containing native SOD or OVO or the corresponding ^{native}PGPFs was not significantly greater than that of bisANS alone (Fig. 3*B*).

^{amorph}PGPFs bind to multiple cell surface receptors and are trafficked to lysosomes

^{amorph}PGPFs were labeled with CF-488 (Biotium; ^{amorph}PGPFs^{488}), purified by size exclusion chromatography, and then incubated with EOC 13.31 or SVEC4-10 cells. When incubated with cells on ice (to inhibit endocytosis), there was measurable binding of ^{amorph}PGPFs^{488} to the surface of both cell types, and this binding could be partially inhibited by a range of inhibitors of cell surface receptors in a cell- and protein-specific manner (Table 1). Lipopolysaccharide (LPS) and methyl-β-cyclodextrin (M-β-CD) significantly inhibited the binding of SOD ^{amorph}PGPFs^{488} to EOC 13.31 cells by ~58 and ~37%, respectively, suggesting that toll-like receptors and lipid rafts may be facilitating cell surface binding. M-β-CD also significantly inhibited the binding of SOD ^{amorph}PGPFs^{488} to SVEC4-10 cells by ~ 23%, again suggesting an involvement of lipid rafts. The binding of OVO ^{amorph}PGPFs^{488} to EOC 13.31 cells was significantly inhibited by receptor-associated protein (RAP), M-β-CD, LPS, and mannan (by ~47, 26, 22, and 19%, respectively), suggesting the involvement of LDL family receptors, lipid rafts, toll-like receptors, and the mannose receptor in the binding. None of the inhibitors tested affected the binding of OVO ^{amorph}PGPFs^{488} to SVEC4-10 cells, indicating that different processes may be involved in this case. In the case of OVO ^{amorph}PGPFs^{488} (but not SOD ^{amorph}PGPFs^{488}), both CLU and A2M partially inhibited binding to both cell types (Fig. 4). CLU inhibited the binding of OVO ^{amorph}PGPFs^{488} to EOC

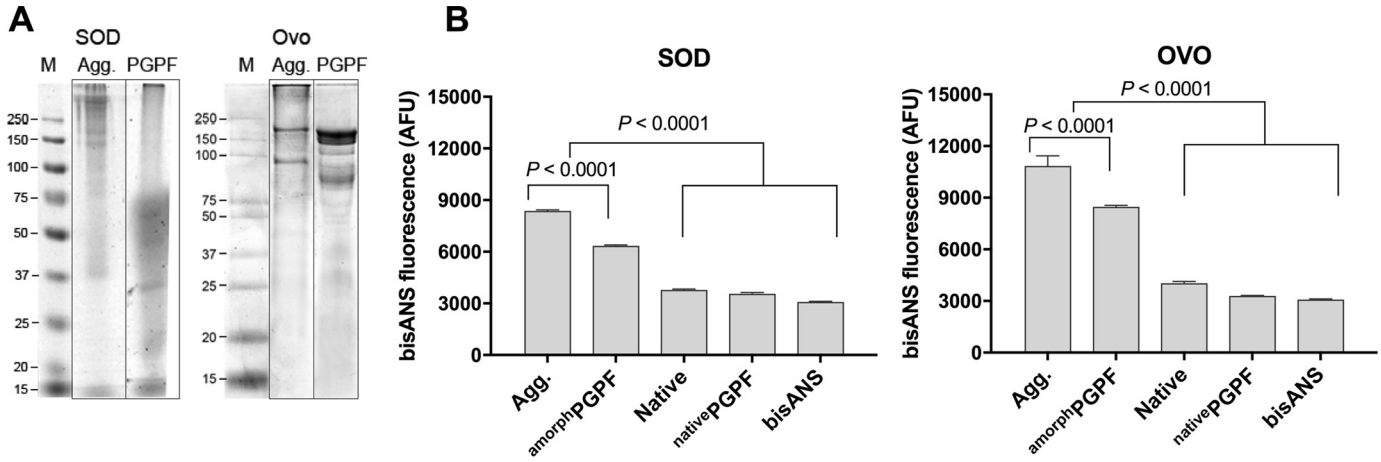

Figure 3. Plm digests amorphous protein aggregates to generate soluble PGPFs that have increased hydrophobicity relative to native proteins. *A*, samples of amorphously aggregated SOD and OVO taken from *in vitro* aggregation assays were diluted in PBS and incubated with or without 100 milliunits of plm overnight at 37 °C to yield PGPFs and undigested aggregates (*Agg.*) respectively, as indicated. Samples were then analyzed under reducing conditions on 12% Tris-Tricine gels and stained with Coomassie Blue. Molecular masses of protein standards are indicated in kDa (*M*). *B*, bisANS-associated fluorescence (*AFU*) was used to measure exposed hydrophobicity for samples of aggregated protein (*Agg.*), ^{amorph}PGPFs, and native protein diluted to 200 μg/ml in PBS. This was compared with ^{native}PGPFs and bisANS alone. *Bars* represent the mean of three independent experiments performed in triplicate ($n = 9$; *error bars* represent S.D.). Significant differences are indicated.

Table 1

Effects of various inhibitors on the binding of ^{amorph}PGPF^{488} to cells at 4 °C

Cells were incubated in ice-cold BSA/PBS/Az for 30 min in the presence or absence of inhibitor and then incubated for a further 30 min in the same buffer containing 20 μg/ml ^{amorph}PGPFs^{488}. Cells were then washed and analyzed by flow cytometry. Mean fluorescence intensity ±S.D. ($n = 9$) of three independent experiments performed in triplicate for each inhibitor is shown. Dashes (—) denote that no significant inhibition was measured. RAP, receptor-associated protein; TLR, toll-like receptor; LDLRs, LDL receptors.

Cell line	^{amorph}PGPF^{488}	Inhibition of binding (inhibitor target)			
		LPS[a] (pan-TLR)	Mannan[a] (mannose receptor)	M-β-CD[b] (lipid rafts)	RAP[c] (LDLRs)
		%			
EOC 13.31	SOD	57.5 ± 7.8	—	37.3 ± 5.8	—
EOC 13.31	OVO	21.5 ± 7.4	19.2 ± 5.2	25.7 ± 0.1	46.9 ± 7.9
SVEC4-10	SOD	—	—	23.3 ± 7.2	—
SVEC4-10	OVO	—	—	—	—

[a] 0.5 μg/ml.
[b] 6.6 mg/ml.
[c] 0.5 mg/ml.

13.31 and SVEC4-10 cells by ~30 and ~34%, respectively, and to SVEC4-10 cells by ~24 and ~35%, respectively. Thus, the results indicate considerable heterogeneity in the mechanism(s) by which PGPFs interact with the cell surface and that, in at least some cases, ECs can partially inhibit the cell surface binding of PGPFs.

When incubated with EOC 13.31 or SVEC4-10 cells at 37 °C for periods of 1–4 h, confocal microscopy analyses showed that both OVO and SOD ^{amorph}PGPFs^{488} were internalized and that the intracellular fluorescence was punctate, consistent with an intravesicular location, and in time overlapped with that of LysoTracker staining (Fig. 4*C*; SVEC4-10 cells shown). A similar pattern of fluorescence was observed for both types of cells stained with LysoTracker following 1–4-h incubation under the same conditions with either fluor-labeled OVO or BSA (not shown). These results are consistent with internalized PGPFs following the classic endocytosis route and being trafficked to lysosomes for degradation.

^{amorph}PGPFs are cytotoxic and are specifically bound by ECs

Colorimetric 3-(4,5-dimethylthiazol-2-yl)-5-(3-carboxymethoxyphenyl)-2-(4-sulfophenyl)-2*H*-tetrazolium (MTS) assays were used to test whether or not ^{amorph}PGPFs and ^{native}PGPFs derived from SOD and OVO and the native parent proteins were cytotoxic to EOC 13.31 and SVEC4-10 cells. For both cell types, ^{amorph}PGPFs derived from SOD and OVO aggregates were toxic. Relative to the PBS only-added control, under the conditions tested, SOD ^{amorph}PGPFs reduced the viability of EOC 13.31 and SVEC4-10 cells by ~72 and ~45%, respectively; the corresponding reductions in viability for OVO ^{amorph}PGPFs were ~44 and ~55%, respectively (Fig. 5). In contrast, in all cases, the viability of cells incubated with ^{native}PGPFs was not significantly different from the control (Fig. 5); the native parent proteins were also not significantly toxic (supplemental Fig. 3). CLU, A2M, and BSA also had no significant effect on cell viability (supplemental Fig. 3). However, the toxicity of ^{amorph}PGPFs was significantly reduced by preincubating them with CLU or A2M and in the case of SOD ^{amorph}PGPFs maintained viable cell numbers at or above that of the control. Preincubation of SOD ^{amorph}PGPFs with CLU actually resulted in a significant increase in viable SVEC4-10 cell numbers above that of the control (Fig. 5*B*). The toxicity of ^{amorph}PGPFs was also confirmed in separate experiments in which dead cells were stained with the membrane-impermeant nucleic acid stain SYTOX Green (supplemental Fig. 4). PGPF preparations had negligible residual plm activity (data not shown), and thus

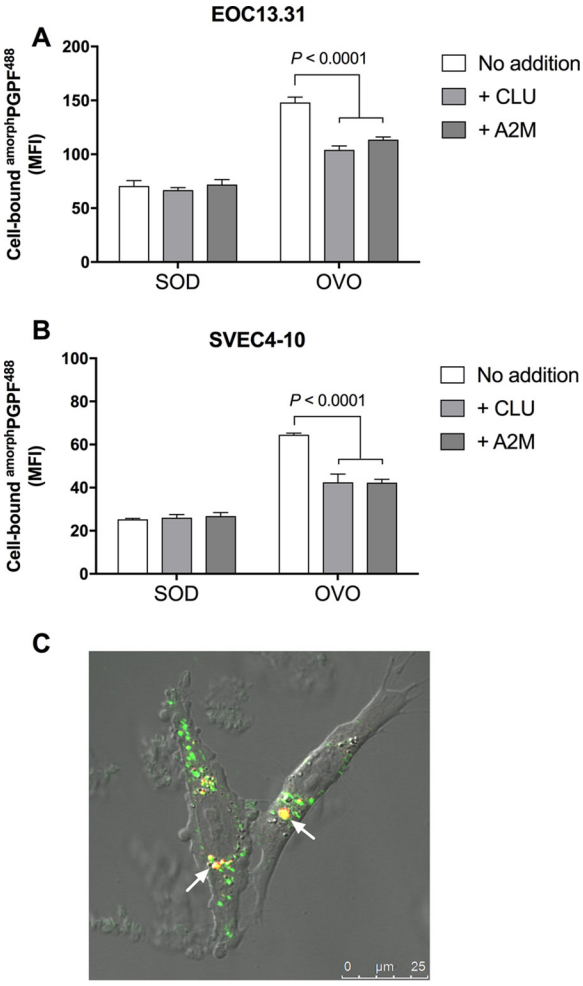

Figure 4. Cell binding and internalization of ^{amorph}PGPFs. EOC 13.31 (*A*) or SVEC4-10 (*B*) cells were incubated for 30 min in the presence or absence of 20 μg/ml SOD or OVO ^{amorph}PGPFs^{488} in ice-cold BSA/PBS/Az following preincubation with or without 100 μg/ml CLU or A2M. Cells were then washed and analyzed by flow cytometry. Results are displayed as the mean fluorescence intensity (*MFI*) of three independent experiments performed in triplicate ($n = 9$; *error bars* represent S.E.). *C*, representative confocal microscope image showing overlay of transmission image, green fluorescence (OVO ^{amorph}PGPFs^{488}), and red fluorescence (LysoTracker Red DND-99) for SCEV4-10 cells following a 2-h incubation with 50 μg/ml OVO ^{amorph}PGPFs^{488}. Areas appearing in *yellow* (*white arrows*) indicate co-localization of internalized ^{amorph}PGPFs^{488} and lysosomes. The *scale bar* indicates 25 μm.

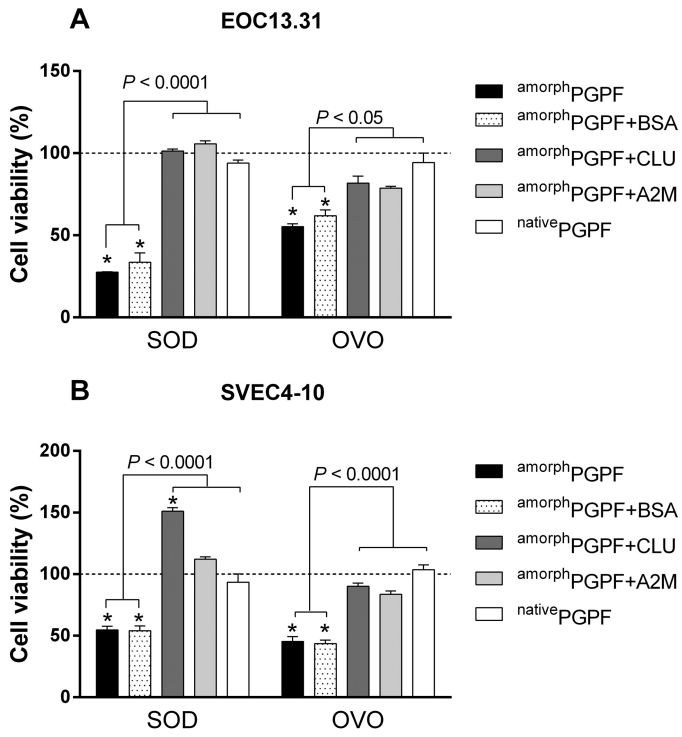

Figure 5. ^{amorph}PGPFs are cytotoxic. Sterile samples of ^{amorph}PGPF or ^{native}PGPF derived from SOD or OVO were preincubated for 1 h at 37 °C in the presence or absence of CLU or A2M or with BSA (non-chaperone control protein) (all proteins at 400 μg/ml) before incubating the PGPFs at a final concentration of 200 μg/ml with EOC 13.31 (*A*) and SVEC4-10 (*B*) cells at 37 °C for 24 h (see *key*). The MTS assay was then performed, and results are plotted as a percentage of the A_{490} for PBS only-added control wells (*dashed line*; see also supplemental Fig. 2). The results are pooled from three independent experiments done in triplicate and are plotted as means ($n = 9$; *error bars* represent S.D.). Significant differences between groups are indicated, and *asterisks above individual bars* indicate that the sample is significantly different from the PBS only-added control (*, $p < 0.001$).

any cytotoxicity measured was attributable to the PGPFs themselves.

Given the demonstrated protective effects of CLU and A2M against the toxicity of ^{amorph}PGPFs, we used a capture ELISA approach to test whether or not ECs bind specifically to ^{amorph}PGPFs. In these assays, specific anti-EC (or control) antibodies were coated onto the microplate wells and subsequently incubated with biotinylated ^{amorph}PGPFs or ^{native}PGPFs that had been preincubated with (or without) ECs. In other controls, antibody-coated ELISA wells were incubated with biotinylated ^{amorph}PGPFs alone or a mixture of these together with BSA as a non-chaperone control protein. If biotinylated species formed complexes with ECs in solution, then the respective anti-EC antibody was expected to specifically capture these complexes from solution. These assays detected significant binding of CLU and A2M to ^{amorph}PGPFs generated from both SOD and OVO but not to the corresponding ^{native}PGPFs. There was also negligible binding detected when wells were incubated with biotinylated ^{amorph}PGPFs alone or a mixture of these with BSA (Fig. 6). Thus, the results indicate that CLU and A2M both specifically bind to ^{amorph}PGPFs to form soluble complexes, and it is likely that this interaction underpins the ability of ECs to protect cells against the toxicity of ^{amorph}PGPFs.

ECs do not interact with PGPFs generated from fibrin

Fibrin clots are not amorphous in structure. On the contrary, thrombin-mediated proteolysis of fibrinogen leads to the assembly of fibrin into a polymer with a very defined and repetitive structure rich in cross-β-sheets (26). The classic fibrinolytic activity of the PAS is known to digest fibrin to yield a number of specific protein fragments of which one, fibrin fragment E, induces apoptosis in various cell types (9). Given our demonstration that ECs specifically bind to and inhibit the toxicity of PGPFs generated from amorphous protein aggregates, we examined whether ECs might also interact with PGPFs generated by the plasmin-mediated digestion of fibrin (*i.e.* ^{fibrin}PGPFs). SDS-PAGE (Fig. 7*A*) analyses of ^{fibrin}PGPF preparations were consistent with previously published studies (13) and the presence of the expected D and E fragments (~95 and ~41–50 kDa, respectively; Fig. 7*A*). Two different ELISA protocols were performed to detect whether or not ^{fibrin}PGPFs

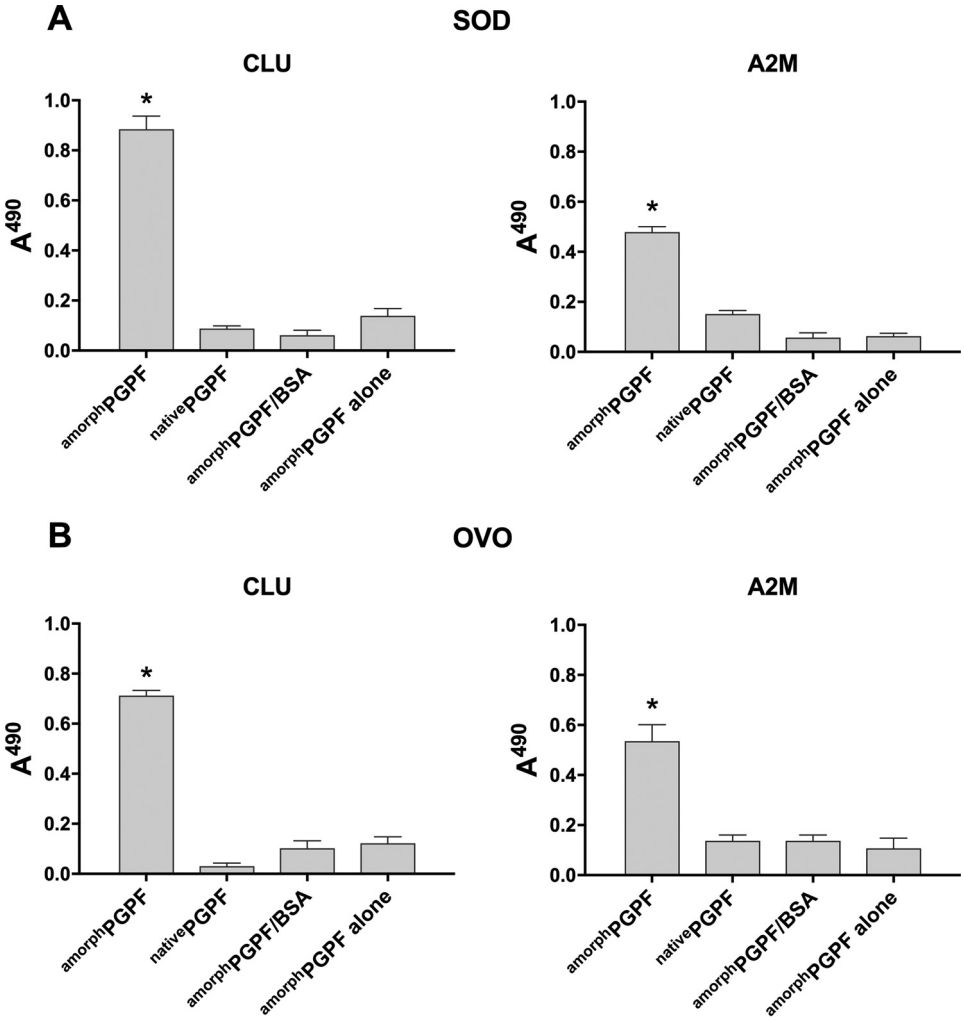

Figure 6. ^{amorph}PGPFs are specifically bound by ECs. Shown are results of capture ELISA in which wells were coated with anti-chaperone or control antibodies and incubated with mixtures of CLU or A2M and biotinylated ^{amorph}PGPFs or ^{native}PGPFs derived from SOD (*A*) or OVO (*B*). Biotinylated proteins subsequently bound to the wells were detected with a complex formed with streptavidin and biotinylated horseradish peroxidase (see "Experimental procedures"). In other controls, antibody-coated ELISA wells were incubated with only biotinylated ^{amorph}PGPFs (*PGPF alone*) or a mixture of this together with BSA as a non-chaperone control protein (*PGPF/BSA*). *Bars* represent the mean of three independent experiments performed in triplicate ($n = 9$; *error bars* represent S.D.; *, $p < 0.001$).

bound to ECs (Fig. 7, *B* and *C*). In the first protocol, purified ECs were immobilized on the plate, and any subsequent binding of biotinylated ^{fibrin}PGPFs was measured (Fig. 7*B*). The second protocol was essentially the same capture assay used previously to demonstrate the formation of EC–^{amorph}PGPFs complexes. Purified anti-EC antibodies were immobilized on the plate and used to capture from solution ECs or any complexes formed between these and biotinylated ^{fibrin}PGPFs during a preincubation step (Fig. 7*C*). No specific binding between ECs and PGPFs was detected using either of the two ELISA protocols. Furthermore, size exclusion chromatographic analysis of ECs, ^{fibrin}PGPFs, and mixtures of ECs and ^{fibrin}PGPFs failed to detect any evidence of the formation of EC–^{fibrin}PGPF complexes (supplemental Fig. 5). Collectively, the results strongly indicate that ECs do not interact with ^{fibrin}PGPFs.

Discussion

Using heat and chemical reduction, we generated aggregates from two model proteins, SOD and OVO, respectively. These aggregates were characterized by thioflavin T assay and electron microscopy as being non-amyloid and physically amorphous in structure. BisANS assays demonstrated that during aggregation the aggregating species showed a time-dependent increase in exposed hydrophobicity. These protein aggregates were shown to act as efficient cofactors for the tPA-mediated activation of plg to plm, producing similar levels of plm activity under the conditions tested as fibrin. Earlier reports had described physically or chemically denatured proteins as stimulating the PAS (15, 17) and established that chemical treatment of these denatured proteins to modify lysine (but not other amino acid) side chains abolished this activity (16). In contrast, lysine residues do not appear to be required for the corresponding activity of amyloid, which instead appears dependent on cross-β structure (27). The current study confirms that cross-β structure is not essential for stimulation of the PAS and that protein aggregates of an apparently entirely amorphous structure are sufficient to stimulate tPA-dependent activation of plm. Furthermore, the demonstration that TXA (a lysine analogue) significantly inhibits the ability of amorphous protein aggregates to elicit plg activation implies that lysine

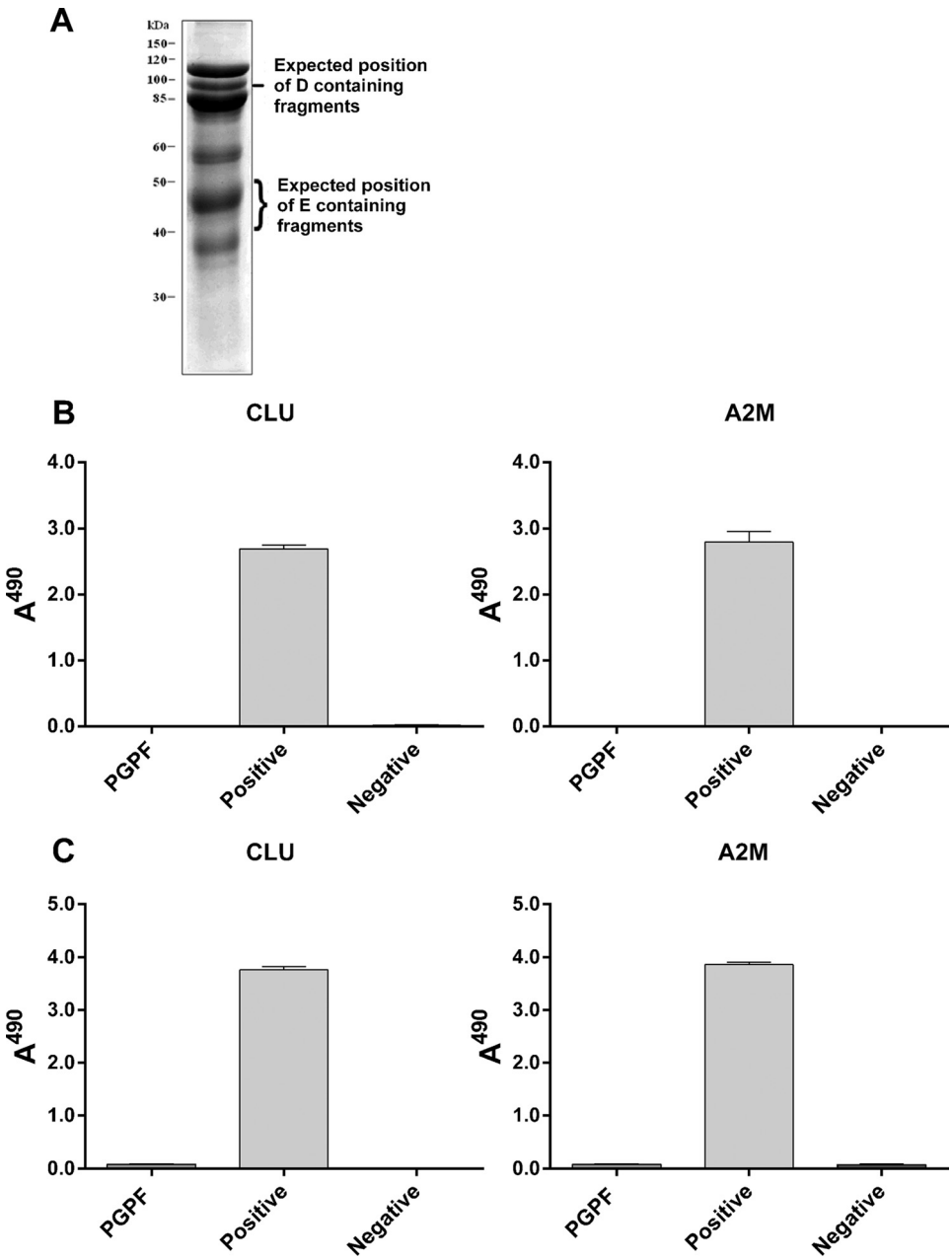

Figure 7. ^{fibrin}PGPFs do not interact with ECs. *A*, image of a Coomassie Blue-stained non-reducing 10% SDS-polyacrylamide gel loaded with ~10 μg of ^{fibrin}PGPFs. Expected positions of fragments containing single D domains (~95 kDa) and E domains (~41–50 kDa) are indicated to the *right*, and positions of molecular mass markers are given on the *left* (mass in kDa). *B* and *C*, histograms showing the results of two ELISA protocols used to detect binding of ECs to ^{fibrin}PGPFs. *B*, binding of biotinylated ^{fibrin}PGFPs (20 μg/ml) to immobilized CLU and A2M. Wells coated with biotinylated PGPFs acted as positive controls, and wells coated with ECs and incubated only with blocking buffer acted as negative controls. *C*, immobilized anti-EC antibodies were used to capture any complexes formed in solution between biotinylated ^{fibrin}PGFPs and CLU or A2M in solution. Wells coated with biotinylated ^{fibrin}PGPFs were used as positive controls, and wells coated with anti-EC antibodies and incubated only with ECs were used as negative controls. Values shown represent the mean ($n = 3$; *error bars* represent S.E.). All absorbance values were corrected for the background control consisting of wells coated only with blocking buffer (HDC/PBS) and then treated as for other corresponding wells.

residues are necessary for the interactions between amorphous protein aggregates and tPA/plg that underpin plg activation (Fig. 2). When end point samples from the amorphous protein aggregation mixtures were separated by centrifugation into fractions designated as soluble and insoluble, both fractions were able to stimulate activation of plg to plm, but these fractions showed a different sensitivity to inhibition by A2AP. The soluble fraction, which would contain smaller protein aggregates that do not pellet during the low-speed centrifugation conditions used, were more sensitive to A2AP inhibition, whereas the larger aggregates present in the centrifugal pellet were significantly more resistant to inhibition by A2AP (Fig. 2). In this respect, the larger, insoluble amorphous aggregates showed a similar resistance to inhibition by A2AP as fibrin, the classic cofactor for the PAS (18).

Digestion of amorphous aggregates of SOD and OVO by plm was efficient and generated smaller, soluble fragments distributed over a broad range of sizes (Fig. 3). During an 8-h incuba-

tion at 37 °C, 100 milliunits of plm generated 3.13 mg of soluble ^{amorph}PGPFs from 4 mg of SOD aggregate in 120 μl (determined using bicinchoninic acid (BCA) assay; not shown). This activity is similar to that reported for the *in vitro* degradation of aggregated Aβ by plm (28). Concentrations of plm used to generate PGPFs from amorphous aggregates (~1.8 μM) were similar to that reported for plg in plasma (1.6–2 μM) (29, 30). Free active plasmin concentrations in human plasma are usually low (~0.02 IU/ml) except in cases of antiplasmin deficiency (31) or thrombolytic therapy (32). The resting cerebrospinal fluid concentrations for plg are reported to be much lower than plasma concentrations (3–15 nM) (33); however, this appears sufficient to allow the degradation of Aβ peptide in mice (34). Additionally, the concentration of plg in cerebrospinal fluid is further increased during breakdown of the blood–brain barrier (33) that occurs, for example, in Alzheimer's disease (35, 36).

Like the parent protein aggregates, relative to the corresponding native proteins, the ^{amorph}PGPFs have relatively high levels of surface-exposed hydrophobicity, which is a characteristic feature of protein species that interact with ECs (37). The levels of bisANS fluorescence measured for ^{amorph}PGPFs approached those of the corresponding undigested aggregates, which are typical of those measured for other unfolded protein samples (38). The binding of CLU and A2M (both ECs) to the ^{amorph}PGPFs was clearly demonstrated by the specific immunocapture of EC–PGPF complexes by immobilized anti-EC antibodies (Fig. 6). When incubated alone with EOC 13.31 or SVEC4-10 cells, the ^{amorph}PGPFs bound by a variety of cell- and protein-specific mechanisms to the cell surface (Table 1). The level of fluorescence measured for cell-associated ^{amorph}PGPF^{488} was of the same order as that previously reported for the binding of fluor-labeled EC–client protein complexes to human peripheral blood cells (39) and in both cases resulted in their progressive internalization into vesicular structures and trafficking to lysosomes, easily detected by confocal microscopy (Fig. 4). Thus, PGPF uptake appears to follow a classic endocytic route.

Notably, when ^{amorph}PGPFs were presented to cells alone, they were significantly cytotoxic. Historically, amorphous protein aggregates have been regarded as generally non-toxic to cells despite their occurrence in many protein deposition diseases. Results presented here, however, show that for both SOD and OVO amorphous aggregates and ^{amorph}PGPFs are cytotoxic, whereas the corresponding native proteins and ^{native}PGPFs are not. This suggests that, as is the case for the toxicity of prefibrillar amyloid-forming oligomers (40–42), the cytotoxicity of amorphous aggregates and the PGPFs derived from them is independent of amino acid sequence and arises instead from a structural or conformational feature. The precise nature of this feature remains to be characterized but is likely to involve regions of exposed hydrophobicity (43). The binding of SOD-derived ^{amorph}PGPFs to cells was less than that of OVO-derived ^{amorph}PGPFs (Fig. 4), but, nevertheless, overall the former appeared to be more cytotoxic (Fig. 5). This is entirely consistent with the observation that amyloid aggregates generated from different proteins have varied levels of cytotoxicity (42, 44), suggesting that the same is true of PGPFs generated from different amorphous protein aggregates.

Under the conditions tested, all (or almost all) of the cytotoxicity was inhibited by preincubation of CLU or A2M with the ^{amorph}PGPFs, whereas the addition of the chaperones to cells in the absence of PGPFs had no significant effect on the numbers of viable cells (Fig. 5 and supplemental Fig. 3). This indicates that, similar to their effects on toxic protein oligomers (45, 46), the formation of soluble complexes between ECs and hydrophobic ^{amorph}PGPFs neutralizes the cytotoxicity of the latter. The reason(s) for the significant increase in viable SVEC4-10 cell numbers, relative to the PBS control, in cultures treated with a preincubated mixture of SOD ^{amorph}PGPFs and CLU (but not CLU alone; Fig. 5*B* and supplemental Fig. 3) is unclear but could result from a cell type-specific proliferative signaling effect of the CLU–^{amorph}PGPFs complexes.

As previously mentioned, the action of plm on fibrin clots also releases PGPFs, which are known to be cytotoxic. However, unlike amorphous protein aggregates, the structure of fibrin is highly ordered, and its digestion by plm releases a relatively small number of fragments corresponding to defined structural elements of the fibrin lattice (Fig. 7*A*). The cytotoxicity of ^{fibrin}PGPF has been identified as arising from a sequence-defined rather than a conformational epitope in fibrin fragment E contained within amino acids 17–104 of the Aα-chain (9). This fundamental difference between ^{amorph}PGPFs and ^{fibrin}PGPFs probably explains why CLU and A2M did not interact with ^{fibrin}PGPFs (Fig. 7*B* and supplemental Fig. 5). ECs and chaperones in general do not bind to specific amino acid sequences but rather bind promiscuously to exposed regions of hydrophobicity on misfolded proteins (47).

Collectively, results presented here and elsewhere show that the PAS satisfies the criteria to play an important role in extracellular proteostasis. Insoluble protein aggregates, whether they are amorphous or amyloid in structure, specifically trigger the PAS to generate active plm, which is able to efficiently degrade the aggregates. Like soluble amyloid oligomers, ^{amorph}PGPFs are cytotoxic, and both types of species have increased hydrophobicity relative to the parent native proteins (48). In both cases, it is likely that ECs bind to these species via regions of exposed hydrophobicity and thereby act to neutralize their toxicity to cells. The toxicity of PGPFs generated by plm-mediated digestion of amyloid fibrils or their interactions with ECs has yet to be tested. ECs have previously been strongly implicated in clearing misfolded proteins from body fluids (1, 39). The current data are consistent with a hypothetical model in which the PAS functionally synergizes with ECs *in vivo*, the PAS first acting to degrade insoluble extracellular protein deposits to release smaller, soluble PGPFs, which are then incorporated into complexes with ECs to neutralize any toxicity and safely transport them in body fluids for subsequent uptake and disposal. This process could be important in clearing and disposing of both proteinaceous debris released during tissue injury (12, 49) and large extracellular protein deposits formed as part of disease pathologies.

It is interesting to note that in the brains of transgenic mice overexpressing human amyloid precursor protein larger and more numerous Aβ plaques were present in heterozygous tPA knock-out mice (homozygous knock-out is fatal) than in control mice (50). Furthermore, relative to controls, $plg^{-/-}$ mice

had elevated levels and delayed clearance of extracellular misfolded tubulin aggregates following neurotrauma (49). Consistent with our hypothetical model, these results suggest that the PAS may have been required for the efficient *in vivo* removal of extracellular protein aggregates in these systems. Future work is required to clarify the potential roles of ECs in these types of important *in vivo* clearance mechanisms and their function in maintaining organismal viability and disease control.

Experimental procedures

Materials

CLU and A2M were purified from human plasma as described previously (51, 52). OVO and all chemicals were obtained from Sigma-Aldrich unless otherwise specified. The G93A mutant of SOD was expressed as a recombinant product in *Escherichia coli* and purified by ammonium sulfate fractionation and size exclusion chromatography as described previously (53).

Protein aggregation assays

Amorphous aggregation of proteins in 96-well microplates (100 μl/well) was monitored by measuring turbidity (changes in absorbance at 360 nm) using a FLUOstar or POLARstar spectrophotometer (BMG Labtech). Proteins were induced to aggregate in PBS (135 mM NaCl, 10 mM Na_2HPO_4, 2.7 mM KCl, 1.75 mM KH_2PO_4, pH 7.4) as follows. OVO (1.5 mg/ml) was heated at 60 °C for 120 min, and SOD (1.4 mg/ml) was incubated with 50 mM DTT and 5 mM EDTA at 37 °C for 24 h. Aggregation mixtures were snap frozen in liquid nitrogen at different time points for use in later experiments.

BisANS and thioflavin T assays

Samples of amorphously aggregated proteins, native proteins, ^{amorph}PGPFs, or nativePGPFs derived at 200 μg/ml; BSA at 300 μg/ml (as a positive control); or no addition (as a negative control) in PBS were supplemented with 100 μM bisANS, and the relative bisANS-associated fluorescence was recorded using a POLARstar spectrophotometer and excitation and emission band pass filters of 355 $\pm$ 5 and 490 $\pm$ 5 nm, respectively. BSA (300 μg/ml) in PBS was used as a positive control for exposed hydrophobicity. Thioflavin T (Thio-T) assays were performed to measure β-sheet structure generated during amyloid aggregation. Samples taken at different time points during protein aggregation assays at a final concentration of 0.75 mg/ml were supplemented with 25 μM Thio-T, and the relative fluorescence was recorded using a POLARstar spectrophotometer and excitation and emission band pass filters of 440 $\pm$ 5 and 490 $\pm$ 5 nm, respectively. BSA (0.75 mg/ml) was used as a negative control. Fibrillar aggregate formed from the SH3 domain of the p85α subunit of bovine phosphatidylinositol 3-kinase was kindly donated by Dr. Justin Yerbury (54) and used as a positive control (also at 0.75 mg/ml).

Scanning electron microscopy

Samples taken from the end points of protein aggregation assays were resuspended at a total protein concentration of 0.1 mg/ml in PBS, and 2 μl of each sample was blotted onto Formvar resin (with carbon coating) nickel mesh grids (Proscitech), incubated for 5 min at room temperature, washed three times with filtered distilled H_2O, and negatively stained with 1% (w/v) uranyl acetate in Milli-Q H_2O for a further 5 min at room temperature. Specimens were examined using a JSM7500FA cold field emission gun scanning electron microscope (JEOL) with an acceleration voltage of 20.0 kV and a working distance of 8 mm (spot size setting of 8).

SDS-PAGE and BCA assays

Protein aggregates and soluble PGPFs were analyzed by 12% resolving Tris-Tricine SDS-PAGE under reducing conditions and stained with Coomassie Blue stain. The molecular weight standards used were from Fermentas. The BCA microplate assay was performed using 384-well plates following the manufacturer's instructions (Sigma); BSA was used as a standard. The concentrations of aggregated protein samples were treated as equivalent to the starting concentration of native protein at the beginning of the corresponding aggregation time course.

Plasminogen activation assays

Samples from protein aggregation assays were dialyzed into HBST (10 mM HEPES, 150 mM NaCl, 0.01% (v/v) Tween 20, pH 7.4). In some experiments, aggregate mixtures were first centrifuged at 15,000 $\times$ *g* for 30 min at 4 °C to separate the mixtures into soluble and insoluble fractions prior to dialysis. The concentration of soluble fractions was determined by BCA assay; the mass concentration of insoluble fractions was estimated by calculating the difference between the protein concentration at the start of the aggregation time course and that of the soluble fraction prepared from the end point of the aggregation mixture. The ability of samples to induce tPA-mediated plg activation to plm was measured as a change in absorbance resulting from the conversion of the plm-specific chromogenic substrate H-D-norleucyl-hexahydrotyrosol-lysine-*para*-nitroanilide diacetate (SPEC-PL; American Diagnostica Inc.) to *para*-nitroaniline. In a 96-well polystyrene microplate (Greiner Bio-one), native or amorphously aggregated protein sample or fibrin (positive control) at an initial concentration of 75 μg/ml in ice-cold HBST (60 μl/well) was incubated with 250 nM plg and 500 nM SPEC-PL in a 96-well polystyrene microplate. Solubilized fibrin stock (25 mg/ml) was prepared according to the manufacturer's instructions (Sigma-Aldrich) and stored aliquoted at −20 °C. The reaction was initiated by adding 10 μl of recombinant human tPA (Actilyse, Roche Applied Science) to a final concentration of 5 nM/well. Absorbance at 405 nm (A_{405}) was measured on a Spectramax Plus 382 plate reader (Molecular Devices) for 120 min at 37 °C with measurements taken at 30-s cycles with 3 s of shaking between cycles. For quantitative analyses, the initial rate of change of plm activity (initial rate of reaction) was calculated from the gradient of the change in A_{405} *versus* t^2 (t^2 was used to linearize the curves and simplify calculation). Data transformation and linear regressions were performed using GraphPad Prism v5.0 (GraphPad Software). In other experiments, the same concentrations as above of tPA, plg, and the protein aggregate sample were first incubated together in HBST for 30 min at 37 °C and then incubated (or not) with 10 mM TXA or 400 nM A2AP for a further 15 min

prior to measuring plm activity. Various background controls were included in all assays including tPA/SPEC-PL, plg/SPEC-PL, SPEC-PL alone, OVO/SPEC-PL, OVO/plg/SPEC-PL, OVO/tPA/SPEC-PL, etc.). The A_{405} associated with these was always small or negligible but was subtracted where appropriate from the raw data.

Plasmin digestion of amorphous protein aggregates

Native proteins were sterilized by filtration through a 0.2-μm-pore-size membrane and induced to aggregate under conditions described above. Samples taken from protein aggregation assays were centrifuged at 15,000 $\times$ *g* for 15 min at 4 °C, and the pellet was resuspended in PBS to ~1 mg/ml. Plm (100 milliunits; Hematologic Technologies, Inc.) was added to 100 μl of the suspended aggregates to give a final total volume of 120 μl and incubated overnight with shaking at 37 °C. Native protein samples were also plm-digested under the same conditions. Insoluble, undigested material was removed by centrifugation at 15,000 $\times$ *g* for 15 min at 4 °C. The concentration of soluble PGPFs in the supernatant was determined by BCA assay. Negligible plasmin activity was measured in PGPF preparations (data not shown).

Conjugation of PGPFs

Biotinylation of PGPFs was performed using biotin-LC-NHS according to the manufacturer's instructions (Thermo Fisher). Unreacted biotin-LC-NHS was removed by dialysis against three changes of PBS, 0.1% azide at 4 °C. PGPFs at ~1 mg/ml in PBS (adjusted to pH 8.3 with 1 M Na_2HCO_3) were incubated with CF-488 SE with gentle shaking for 1 h at room temperature while protected from light. Unreacted CF-488 was subsequently removed by size exclusion chromatography, and the concentrations of CF-488-conjugated PGPFs ($PGPFs^{488}$) were subsequently determined using a BCA assay.

ELISA

For direct binding ELISA, plates (384-well) were coated with 10 μg/ml purified human clusterin or A2M. Unless otherwise indicated, all additions to wells were of 30-μl volumes, incubations were for 1 h at 37 °C, and wash steps were performed with shaking; plates were washed six times with PBS containing 0.1% (v/v) Tx-100 (Tx-100/PBS) followed by six washes with PBS. Wells were then blocked with 50 μl/well 1% (w/v) heat-denatured casein in PBS (HDC/PBS) before incubating with 20 μg/ml biotinylated PGPFs in HDC/PBS. Following washing, bound biotinylated proteins were detected using a mixture of 2.5 μg/ml each of streptavidin and biotinylated HRP in HDC/PBS. Finally, color was developed with the addition of 30 μl/well 2.5 mg/ml *o*-phenylenediamine dihydrochloride in 50 mM dibasic sodium phosphate, 25 mM citric acid, pH 5.0, supplemented with 0.03% (w/v) H_2O_2 and incubation for 5 min at room temperature, and the reaction was stopped with the addition of 30 μl/well 1 M HCl. For capture ELISA, wells were first coated with 10 μg/ml G7 anti-CLU monoclonal antibody, mouse anti-human A2M monoclonal antibody (Abcam, ab58703), or isotype control antibody (mouse IgG1κ antibody; Millipore) in PBS and then blocked as above. Before incubating on the blocked plate, biotinylated PGPFs at 50 μg/ml in 1% (w/v) BSA in Tx-100/PBS were preincubated for 1 h at 37 °C with or without 20 μg/ml CLU or A2M or with BSA (as a non-chaperone control protein). Bound biotinylated proteins were detected as above. For all ELISAs, the A_{490} was measured using a Spectramax Plus 382 plate reader. Absorbances from wells coated with isotype control antibody were subtracted from corresponding wells coated with G7 anti-CLU and anti-A2M antibodies.

Cell culture

EOC 13.31 (microglial-like), SVEC4-10 (endothelial-like), and LADMAC (monocyte-like) murine cell lines were obtained from the American Type Culture Collection. Cell lines were grown in DMEM/F-12 (Life Technologies) containing 10% (v/v) fetal calf serum (FCS) at 37 °C and 5% CO_2 and subcultured when they reached 80% confluence. EOC 13.31 cells were additionally supplemented with 20% (v/v) LADMAC-conditioned medium (which contains secreted colony-stimulating factor-1). For experiments involving the addition of chaperones, in an effort to limit the effects of bovine chaperones that may be present in the FCS, cells were incubated with treatments in DMEM/F-12 containing only 1% (v/v) FCS.

Binding of PGPFs to cells

EOC 13.31 and SVEC4-10 cells were harvested using StemPro Accutase (Life Technologies) (which does not cleave cell surface proteins) and resuspended in ice-cold 1% (w/v) BSA, PBS, 0.1% (w/v) NaN_3 (BSA/PBS/Az). $PGPFs^{488}$ were preincubated with or without CLU or A2M in PBS for 1 h at 37 °C (all proteins at 400 μg/ml) before diluting to a final concentration of 20 μg/ml in BSA/PBS/Az and incubating with cells for 30 min on ice. In other experiments, cells were preincubated for 30 min in ice-cold BSA/PBS/Az, with or without each of the specific inhibitors shown in Table 1, before incubating with $PGPFs^{488}$ as before. Following incubations, cells were washed and resuspended in BSA/PBS/Az before flow cytometric analysis; cells incubated only in BSA/PBS/Az were used as the negative control in these assays. Non-viable cells were stained with 1 μM propidium iodide and excluded from analyses by electronic gating. Flow cytometry was performed using a Fortessa X-20 instrument and FACSDiva v8.0 acquisition software (BD Biosciences). Fluorescence was collected using excitation at 488 nm and emissions at 525 $\pm$ 25 nm (CF-488) and 695 $\pm$ 20 nm (propidium iodide). Data analysis was performed using FlowJo software (v10.2 for Macintosh; FlowJo, LLC).

Confocal microscopy

Cells were grown in 8-chamber μ-slides (Ibidi). LysoTracker Red DND-99 (50 nM; Invitrogen) and $PGPFs^{488}$ (20–100 μg/ml) were added to the slide chambers and incubated for 1–4 h before washing with phenol red-free DMEM/F-12. Images for $PGPF^{488}$ and LysoTracker Red DND-99 fluorescence were then collected sequentially using an inverted Leica SP5 confocal microscope (Leica Microsystems, Sydney, Australia). Excitation lasers and emission collection windows used were, respectively, 488 and 510–580 nm for $PGPFs^{488}$ and 561 and 600–700 nm for LysoTracker Red DND-99. A transmission image was also collected using the 488 nm laser as the light source.

Cell viability assays

PGPFs were preincubated with or without CLU or A2M or with BSA as a non-chaperone control protein in PBS for 1 h at 37 °C (all proteins present at 1 mg/ml). They were then added to cultures of EOC 13.31 or SVEC4-10 cells such that each protein added had a final concentration of 200 μg/ml and incubated for 24–90 h at 37 °C and 5% (v/v) CO_2. The MTS assay was performed using a CellTiter 96 AQ_{ueous} One Solution Cell Proliferation Assay kit (Promega) by adding 20 μl/well MTS reagent and incubating for 2 h at 37 °C before measuring the A_{490} using a Spectramax Plus 382 plate reader. Real-time SYTOX Green assays were performed by incubating cells with 1 μM SYTOX Green viability dye (Life Technologies) and measuring the development of SYTOX Green-associated fluorescence over 72 h by time-resolved epifluorescence microscopy (excitation at 440–480 nm, emission at 504–544 nm) using an Incucyte ZOOM epifluorescence live-cell imaging system (Essen Bioscience; Nikon 4× objective). Data were analyzed using Incucyte ZOOM software v2015A.

Statistical analysis

Data presented were analyzed by one-way analysis of variance with Tukey's multiple comparison post-test or two-way analysis of variance with Holm-Sidak multiple comparison post-test using GraphPad Prism v6.00 for Windows.

Author contributions—P. C., R. A. B., and A. R. W. performed all experiments and interpreted data. P. C. also contributed to authoring of the manuscript. M. R. W. was the coordinating author with significant input from M. R., and M. R. W. and M. R. also designed experiments and interpreted data.

Note added in proof—In the version of this article that was published as a Paper in Press on July 14, 2017, Fig. 3A did not indicate the borders between different sections of a gel. This error has now been corrected and does not affect the results or conclusions of this work.

References

1. Wyatt, A. R., Yerbury, J. J., Ecroyd, H., and Wilson, M. R. (2013) Extracellular chaperones and proteostasis. *Annu. Rev. Biochem.* **82,** 295–322
2. Gillmore, J. D., and Hawkins, P. N. (2006) Drug insight: emerging therapies for amyloidosis. *Nat. Clin. Pract. Nephrol.* **2,** 263–270
3. Danø, K., Behrendt, N., Høyer-Hansen, G., Johnsen, M., Lund, L. R., Ploug, M., and Rømer, J. (2005) Plasminogen activation and cancer. *Thromb. Haemost.* **93,** 676–681
4. Ranson, M., and Andronicos, N. (2003) Plasminogen binding and cancer: promises and pitfalls. *Front. Biosci.* **8,** s294–304
5. Gilabert, J., Estelles, A., Grancha, S., Espana, F., and Aznar, J. (1995) Fibrinolytic system and reproductive process with special reference to fibrinolytic failure in pre-eclampsia. *Hum. Reprod.* **10,** Suppl. 2, 121–131
6. Clemmensen, I., and Andersen, R. B. (1982) The fibrinolytic system and its relation to inflammatory diseases. *Semin. Arthritis Rheum.* **11,** 390–398
7. Mathias, M., and Leisner, R. (2007) Understanding haemostasis. *Paediatr. Child Health* **17,** 317–321
8. Cesarman-Maus, G., and Hajjar, K. A. (2005) Molecular mechanisms of fibrinolysis. *Br. J. Haematol.* **129,** 307–321
9. Guo, Y. H., Hernandez, I., Isermann, B., Kang, T. B., Medved, L., Sood, R., Kerschen, E. J., Holyst, T., Mosesson, M. W., and Weiler, H. (2009) Caveolin-1-dependent apoptosis induced by fibrin degradation products. *Blood* **113,** 4431–4439
10. Tucker, H. M., Kihiko-Ehmann, M., Wright, S., Rydel, R. E., and Estus, S. (2000) Tissue plasminogen activator requires plasminogen to modulate amyloid-β neurotoxicity and deposition. *J. Neurochem.* **75,** 2172–2177
11. Kranenburg, O., Bouma, B., Kroon-Batenburg, L. M., Reijerkerk, A., Wu, Y. P., Voest, E. E., and Gebbink, M. F. (2002) Tissue-type plasminogen activator is a multiligand cross-β structure receptor. *Curr. Biol.* **12,** 1833–1839
12. Samson, A. L., Borg, R. J., Niego, B., Wong, C. H., Crack, P. J., Yongqing, T., and Medcalf, R. L. (2009) A nonfibrin macromolecular cofactor for tPA-mediated plasmin generation following cellular injury. *Blood* **114,** 1937–1946
13. Mosesson, M. W., Siebenlist, K. R., Amrani, D. L., and DiOrio, J. P. (1989) Identification of covalently linked trimeric and tetrameric D domains in crosslinked fibrin. *Proc. Natl. Acad. Sci. U.S.A.* **86,** 1113–1117
14. Ellis, V., Daniels, M., Misra, R., and Brown, D. R. (2002) Plasminogen activation is stimulated by prion protein and regulated in a copper-dependent manner. *Biochemistry* **41,** 6891–6896
15. Machovich, R., and Owen, W. G. (1997) Denatured proteins as cofactors for plasminogen activation. *Arch. Biochem. Biophys.* **344,** 343–349
16. Radcliffe, R. (1983) A critical role of lysine residues in the stimulation of tissue plasminogen activator by denatured proteins and fibrin clots. *Biochim. Biophys. Acta* **743,** 422–430
17. Radcliffe, R., and Heinze, T. (1981) Stimulation of tissue plasminogen activator by denatured proteins and fibrin clots: a possible additional role for plasminogen activator? *Arch. Biochem. Biophys.* **211,** 750–761
18. Suenson, E., Lützen, O., and Thorsen, S. (1984) Initial plasmin-degradation of fibrin as the basis of a positive feed-back mechanism in fibrinolysis. *Eur. J. Biochem.* **140,** 513–522
19. Abdolvahabi, A., Shi, Y., Chuprin, A., Rasouli, S., and Shaw, B. F. (2016) Stochastic formation of fibrillar and amorphous superoxide dismutase oligomers linked to amyotrophic lateral sclerosis. *ACS Chem. Neurosci.* **7,** 799–810
20. Yerbury, J. J., Rybchyn, M. S., Easterbrook-Smith, S. B., Henriques, C., and Wilson, M. R. (2005) The acute phase protein haptoglobin is a mammalian extracellular chaperone with an action similar to clusterin. *Biochemistry* **44,** 10914–10925
21. Collen, D. (1976) Identification and some properties of a new fast-reacting plasmin inhibitor in human plasma. *Eur. J. Biochem.* **69,** 209–216
22. Collen, D., and Wiman, B. (1978) Fast-acting plasmin inhibitor in human plasma. *Blood* **51,** 563–569
23. Lijnen H. R., and Collen, D. (1982) Interaction of plasminogen activators and inhibitors with plasminogen and fibrin. *Semin. Thromb. Hemost.* **8,** 2–10
24. Lijnen, H. R., Maes, M., Castel, M., Samama, M., and Collen, D. (1982) Kinetics of the inhibition of plasmin in acidified human plasma. *Thromb. Haemost.* **48,** 257–259
25. Wu, H. L., Shi, G. Y., and Bender, M. L. (1987) Preparation and purification of microplasmin. *Proc. Natl. Acad. Sci. U.S.A.* **84,** 8292–8295
26. Gebbink, M. F. (2011) Tissue-type plasminogen activator-mediated plasminogen activation and contact activation, implications in and beyond haemostasis. *J. Thromb. Haemost.* **9,** 174–181
27. Beringer, D. X., Fischer, M. J., Meeldijk, J. D., van Donselaar, E. G., de Mol, N. J., and Kroon-Batenburg, L. M. (2013) Tissue-type plasminogen activator binds to Aβ and AIAPP amyloid fibrils with multiple domains. *Amyloid* **20,** 113–121
28. Tucker, H. M., Kihiko, M., Caldwell, J. N., Wright, S., Kawarabayashi, T., Price, D., Walker, D., Scheff, S., McGillis, J. P., Rydel, R. E., and Estus, S. (2000) The plasmin system is induced by and degrades amyloid-β aggregates. *J. Neurosci.* **20,** 3937–3946
29. Kwaan, H. C. (1992) The plasminogen-plasmin system in malignancy. *Cancer Metastasis Rev.* **11,** 291–311
30. Cederholm-Williams, S. A. (1981) Concentration of plasminogen and antiplasmin in plasma and serum. *J. Clin. Pathol.* **34,** 979–981
31. Carpenter, S. L., and Mathew, P. (2008) α_2-Antiplasmin and its deficiency: fibrinolysis out of balance. *Haemophilia* **14,** 1250–1254
32. Stief, T. W., Richter, A., Bünder, R., Maisch, B., and Renz, H. (2006) Monitoring of plasmin and plasminogen activator activity in blood of patients

under fibrinolytic treatment by reteplase. *Clin. Appl. Thromb. Hemost.* **12,** 213–218
33. Mezzapesa, A., Orset, C., Plawinski, L., Doeuvre, L., Martinez de Lizarrondo, S., Chimienti, G., Vivien, D., Mansour, A., Matà, S., Pepe, G., and Anglés-Cano, E. (2014) Plasminogen in cerebrospinal fluid originates from circulating blood. *J. Neuroinflammation* **11,** 154
34. Melchor, J. P., Pawlak, R., and Strickland, S. (2003) The tissue plasminogen activator-plasminogen proteolytic cascade accelerates amyloid-β (Aβ) degradation and inhibits Aβ-induced neurodegeneration. *J. Neurosci.* **23,** 8867–8871
35. Yamada, M. (2000) Cerebral amyloid angiopathy: an overview. *Neuropathology* **20,** 8–22
36. Jellinger, K. A. (2002) Alzheimer disease and cerebrovascular pathology: an update. *J. Neural Transm.* **109,** 813–836
37. Poon, S., Rybchyn, M. S., Easterbrook-Smith, S. B., Carver, J. A., Pankhurst, G. J., and Wilson, M. R. (2002) Mildly acidic pH activates the extracellular molecular chaperone clusterin. *J. Biol. Chem.* **277,** 39532–39540
38. Wyatt, A. R., Yerbury, J. J., and Wilson, M. R. (2009) Structural characterization of clusterin-chaperone client protein complexes. *J. Biol. Chem.* **284,** 21920–21927
39. Wyatt, A. R., Yerbury, J. J., Berghofer, P., Greguric, I., Katsifis, A., Dobson, C. M., and Wilson, M. R. (2011) Clusterin facilitates *in vivo* clearance of extracellular misfolded proteins. *Cell. Mol. Life Sci.* **68,** 3919–3931
40. Chiti, F., and Dobson, C. M. (2006) Protein misfolding, functional amyloid, and human disease. *Annu. Rev. Biochem.* **75,** 333–366
41. Stefani, M., and Dobson, C. M. (2003) Protein aggregation and aggregate toxicity: new insights into protein folding, misfolding diseases and biological evolution. *J. Mol. Med.* **81,** 678–699
42. Bucciantini, M., Giannoni, E., Chiti, F., Baroni, F., Formigli, L., Zurdo, J., Taddei, N., Ramponi, G., Dobson, C. M., and Stefani, M. (2002) Inherent toxicity of aggregates implies a common mechanism for protein misfolding diseases. *Nature* **416,** 507–511
43. Mannini, B., Cascella, R., Zampagni, M., van Waarde-Verhagen, M., Meehan, S., Roodveldt, C., Campioni, S., Boninsegna, M., Penco, A., Relini, A., Kampinga, H. H., Dobson, C. M., Wilson, M. R., Cecchi, C., and Chiti, F. (2012) Molecular mechanisms used by chaperones to reduce the toxicity of aberrant protein oligomers. *Proc. Natl. Acad. Sci. U.S.A.* **109,** 12479–12484
44. Yerbury, J. J., Poon, S., Meehan, S., Thompson, B., Kumita, J. R., Dobson, C. M., and Wilson, M. R. (2007) The extracellular chaperone clusterin influences amyloid formation and toxicity by interacting with prefibrillar structures. *FASEB J.* **21,** 2312–2322
45. Narayan, P., Ganzinger, K. A., McColl, J., Weimann, L., Meehan, S., Qamar, S., Carver, J. A., Wilson, M. R., St George-Hyslop, P., Dobson, C. M., and Klenerman, D. (2013) Single molecule characterization of the interactions between amyloid-β peptides and the membranes of hippocampal cells. *J. Am. Chem. Soc.* **135,** 1491–1498
46. Cascella, R., Conti, S., Tatini, F., Evangelisti, E., Scartabelli, T., Casamenti, F., Wilson, M. R., Chiti, F., and Cecchi, C. (2013) Extracellular chaperones prevent Aβ-induced toxicity in rat brains. *Biochim. Biophys. Acta* **1832,** 1217–1226
47. Gething, M. J. (1996) Molecular chaperones: clasping the prize. *Curr. Biol.* **6,** 1573–1576
48. Bolognesi, B., Kumita, J. R., Barros, T. P., Esbjorner, E. K., Luheshi, L. M., Crowther, D. C., Wilson, M. R., Dobson, C. M., Favrin, G., and Yerbury, J. J. (2010) ANS binding reveals common features of cytotoxic amyloid species. *ACS Chem. Biol.* **5,** 735–740
49. Samson, A. L., Knaupp, A. S., Sashindranath, M., Borg, R. J., Au, A. E., Cops, E. J., Saunders, H. M., Cody, S. H., McLean, C. A., Nowell, C. J., Hughes, V. A., Bottomley, S. P., and Medcalf, R. L. (2012) Nucleocytoplasmic coagulation: an injury-induced aggregation event that disulfide cross-links proteins and facilitates their removal by plasmin. *Cell Rep.* **2,** 889–901
50. Oh, S. B., Byun, C. J., Yun, J. H., Jo, D. G., Carmeliet, P., Koh, J. Y., and Lee, J. Y. (2014) Tissue plasminogen activator arrests Alzheimer's disease pathogenesis. *Neurobiol. Aging* **35,** 511–519
51. Yerbury, J. J., Kumita, J. R., Meehan, S., Dobson, C. M., and Wilson, M. R. (2009) α_2-Macroglobulin and haptoglobin suppress amyloid formation by interacting with prefibrillar protein species. *J. Biol. Chem.* **284,** 4246–4254
52. Humphreys, D. T., Carver, J. A., Easterbrook-Smith, S. B., and Wilson, M. R. (1999) Clusterin has chaperone-like activity similar to that of small heat-shock proteins. *J. Biol. Chem.* **274,** 6875–6881
53. Roberts, K., Zeineddine, R., Corcoran, L., Li, W., Campbell, I. L., and Yerbury, J. J. (2013) Extracellular aggregated Cu/Zn superoxide dismutase activates microglia to give a cytotoxic phenotype. *Glia.* **61,** 409–419
54. Kumita, J. R., Poon, S., Caddy, G. L., Hagan, C. L., Dumoulin, M., Yerbury, J. J., Stewart, E. M., Robinson, C. V., Wilson, M. R., and Dobson, C. M. (2007) The extracellular chaperone clusterin potently inhibits human lysozyme amyloid formation by interacting with prefibrillar species. *J. Mol. Biol.* **369,** 157–167

Amorphous protein aggregates stimulate plasminogen activation, leading to release of cytotoxic fragments that are clients for extracellular chaperones

Patrick Constantinescu, Rebecca A. Brown, Amy R. Wyatt, Marie Ranson and Mark R. Wilson

J. Biol. Chem. 2017, 292:14425-14437.
doi: 10.1074/jbc.M117.786657 originally published online July 14, 2017